Pinelli, A., Omidyeganeh, M., Brücker, C., Revell, A., Sarkar, A. & Alinovi, E. (2016). The PELskin project: part IV—control of bluff body wakes using hairy filaments. Meccanica, doi: 10.1007/s11012-016-0513-0

CITY UNIVERSITY LONDON

EST 1894

City Research Online

CrossMark

The PELskin project: part IV—control of bluff body wakes using hairy filaments

**Alfredo Pinelli · Mohammad Omidyeganeh · Christoph Brücker ·
Alistair Revell · Abhishek Sarkar · Edoardo Alinovi**

Abstract The passive control of bluff body wakes using a sparse layer of elastic hairy filaments has been investigated via a series of numerical simulations and compared to selected experiments under well-controlled boundary conditions. It has been found that a distribution of filaments spaced half of the dominant three dimensional instability and resonating with the main shedding frequency can drastically delay the three dimensional transition of the wake behind a circular cylinder. It will also be shown that when using a pair of rows of filaments symmetrically spaced by an azimuthal angle, the wake topology can be deeply affected as well as the value of the integral force coefficients of the cylinder. In the most favourable case, a coupled three dimensional transition delay and strongly reduced values of the drag and of the lift fluctuation can be simultaneously achieved. These results hold also for higher Reynolds-number flows as shown in experiments on a cylinder with hairy flaps attached to the aft part. The lock-in effect of structural vibration of the flaps with the vortex shedding is assumed to be the reason for a sudden change in the shedding cycle as soon as the motion amplitude is high enough to modify the wake. In line with this hypothesis, it has been demonstrated that a long elastic filament pinned on the centerline of a forced spatially developing mixing layer can interact with the vortex dynamics delaying the pairing process-leading to a reduced thickness of the layer. These findings show that a properly designed fluid structure interaction can indeed lead to technological benefits in terms of wake control: drag reduction, vibration control and possibly palliation of aeroacoustic emissions.

Keywords Bluff body wake · Hairy filaments · Immersed boundary

A. Pinelli · M. Omidyeganeh (✉) · C. Brücker
Department of Mechanical and Aeronautical Engineering,
City, University of London, London, UK
e-mail: omid.yeganeh@city.ac.uk

A. Pinelli
e-mail: Alfredo.Pinelli.1@city.ac.uk

A. Revell · A. Sarkar
Department of Mechanical Engineering, Manchester
University, Manchester, UK

E. Alinovi
Dipartimento di Ingegneria Civile, Chimica ed
Ambientale, Universitá di Genova, Genoa, Italy

1 Introduction

The results that will be presented in this manuscript have been obtained in the framework of the EU financed project *Pelskin* (7th Framework Programme of the European Commission). The general motivation of the Project has been the exploration of passive control techniques based on self adaptive devices that react dynamically to the actual flow conditions via

fluid structure interactions. On one hand, these interactions lead to a continuous variations of the boundary conditions seen by the fluid. On the other, the force exerted by the fluid on the elastic devices lead to a dynamic reconfiguration of the flow geometric boundaries. In particular, the present contribution focuses on the use of a sparse set of hairy elastic filaments interfering with large vortical structures that are generated in the wakes of bluff bodies or as a result of a basic linear instability like in the case of a forced mixing layer. The filaments reconfiguration should promote a reduction in form drag by decreasing the thickness of the wake and the mixing layer or by altering the pressure distribution around immersed bodies in the fluid. In particular, controlling vortex shedding would lead to a palliation of the unsteady pressure drops taking place on the rear part of the body. The consequent reduction of forces fluctuations should also be beneficial as it could have an impact in reducing structural vibrations and eventually sound generation. Due to the practical importance of those considerations in many engineering problems, much attention has been devoted to manipulate vortex shedding with active and/or passive means. Among them, attaching a splitter plate to the cylinder base has been known to be one of the most successful ways for controlling vortex shedding. Known effects of the splitter plate on the wake are: shedding frequency decreases non-monotonically with the change of the length of the splitter plate; the critical length l_c of the plate (non dimensionalised with the cylinder diameter D) at which shedding disappears scales linearly with the Reynolds number ($Re_D = U_\infty D/\nu$, U_∞ being the free stream velocity and ν the kinematic viscosity); the critical length l_c corresponds the separation bubble length in the unmodified case [7]. While several numerical and experimental studies considered rigid and not deformable splitter plates for controlling vortex shedding, the effects of the flexibility of a splitter plate on the modification of vortex shedding behind a bluff body have not been studied extensively until recently. The present interest in the use of flexible splitter plates has been mainly motivated for its potential use as an energy harvesting device. Taylor et al. [17] and Allen and Smits [1] examined the potential use of a flexible splitter plate, which is made of a piezoelectric membrane, attached to a bluff body for generation of electricity from vortex-shedding-induced vibration of the plate. Flexible membranes

have been considered recently by Mazellier et al. [11] to control the wake generated behind a square cylinder. In particular, their device consisting of a couple of flaps made from the combination of a rigid plastic skeleton coated with a porous fabric mimicking the shaft and the vane of the birds feathers, led to a net drag reduction of about 22 %. At the same time, experimental studies on circular cylinders with hairy flaps on it proved that these flaps are able to modify the shedding cycle [9]. The study showed a characteristic jump in the shedding frequency at a critical Reynolds number of $Re_c \approx 14,000$ when comparing to the classical behaviour of a plain cylinder wake flow. The analysis of the motions of the hairy-flaps showed that for $Re = Re_c$ the amplitude of the flap motion is considerably increased and a characteristic travelling wave-like motion pattern could be observed along the row of flaps. As a consequence the presence of the hairy flaps alter the phase within the vortex shedding cycle such that the transversal dislocation (transversal distance from the centerline) of the shed vortices is reduced [9]. Accordingly, the vortices are not arranged in a classical zig-zag pattern of the Kármán vortex-street, rather they are shed in a row along the centerline.

Despite increasing engineering interest, the quantitative relationship between the characteristics of shed vortices and the material and geometric properties of a splitter plate, which describes the gross influence on the drag and lift of the bluff body and the vibration of the plate, is not well understood and has not been explored in details for achieving different technological benefits. This lack of knowledge is particularly severe in the case of the flow around three dimensional slender elastic filaments, for which no information is available in the literature except the results that have been obtained by the PELskin consortium. In this framework, the present study aimed at conducting an extensive investigation of the effects of the flexibility and the length of one or two splitter flexible plates (i.e., in a two dimensional configuration) on the drag and lift of a cylinder and vibration of the plate using numerical methods. The investigation has also been extended to a genuinely three dimensional case showing that it is possible to delay or even cancel the spanwise instabilities of the wake behind a cylinder using a set of properly spaced flexible tiny filaments located on the lee side of the cylinder. To further highlight the potential for passive

flow control of wakes, we have also considered the canonical case of a two dimensional forced mixing layer.

All the results in this manuscript have been obtained using a computational methodology that combines an immersed-boundary method, which is capable of simulating flow over non-grid-conforming complex moving bodies and a Euler–Bernoulli unsteady beam model. The experimental work that has been designed to validate the numerical method will also be described together with the quantitative results that have been used for the cross comparison between numerical predictions and experimental data.

The next section will provide details of the computational methodology and of its validation through simulations of a benchmark experiment. It will be followed by the description and by the results that have been obtained in the two dimensional settings: first for a filament interacting with a forced mixing layer and later on for the wake manipulation of the cylinder with appended elastic flaps case. The extension to flow control of the three dimensional wake behind a cylinder will then follow. Finally some conclusions and perspectives will be drawn.

2 Numerical methodology

The numerical campaign has been carried out considering the unsteady, incompressible Navier–Stokes equations:

$$\frac{\partial u_i}{\partial t} + \frac{\partial u_i u_j}{\partial x_j} = -\frac{\partial P}{\partial x_i} + \frac{1}{Re_D}\nabla^2 u_i + f_i, \quad \frac{\partial u_i}{\partial x_i} = 0,$$

(1)

where the Einstein convention on summation indices applies ($i, j = 1, 2$, or $i, j = 1, 2, 3$, for two or three-dimensional cases, respectively), $Re_D = U_\infty D / v$ (unless stated otherwise D is the cylinder diameter, U_∞ is the approaching velocity magnitude, and v is the kinematic viscosity). The following notations will also been used: $x_1 - u_1$(or $x - u$) stand for the streamwise direction and the streamwise velocity component, $x_2 - u_2$ (or $y - v$) are used for the normal direction and velocity components, and $x_3 - u_3$ (or $z - w$) are used for three dimensional case to indicate the spanwise direction and velocity component. The governing differential Eq. (1) are discretised on a non-staggered

grid using a curvilinear second order centered finite-volume code. The temporal advancement is performed with a second-order-accurate semi-implicit fractional-step procedure, where Crank–Nicolson scheme is used for the diffusive terms, and the Adams–Bashforth scheme for all the other terms. The solenoidal condition on the velocity field is enforced by a Poisson equation for the pressure, which is solved via a fast Poisson solver. Further details on the code, its parallelization and the extensive validation campaign can be found in [13]. The presence of immersed rigid bodies inside the domain is kept into account using a classical direct immersed boundary method [4], while the boundary conditions on the deforming boundaries (i.e., the flexible splitter plates and the filaments) are enforced by using an original immersed boundary method developed by some of the authors of the present manuscript. For the sake of completeness we will shortly summarise the immersed boundary method methodology applied to the deforming boundaries. For further details the interested reader can refer to [5, 15] and "The PELskin project—part I—Fluid–structure interaction for a row of flexible flaps: a reference study in oscillating channel flow" by Li et al. in this issue.

2.1 Elastic flaps and filaments model

We consider a flexible filament-like structure of length L, linear density ρ_s, immersed in a fluid of density ρ_f and subject to a gravitational acceleration $\mathbf{g}$. The filament is discretised using a set of Lagrangian markers located at coordinates $\mathbf{X}$s. Also, we associate to each marker a discrete force $\mathbf{F}_{ib}$ representing the force exerted by the filament on the fluid (also defined on each marker). The latter, as already explained, is related to its Eulerian counterpart by the convolution with a Dirac's function over a volume Ω given by:

$$\mathbf{F}_{ib}(\mathbf{X}) = \int_\Omega \mathbf{f}_{ib}(\mathbf{x})\tilde{\delta}(\mathbf{x} - \mathbf{X})dV$$

(2)

We will also use the following notations: E refers to the Young's modulus of the filament, I is the moment of inertia of the filament ($K_B = EI$ the flexural rigidity of the filament), and T the tension within the filament. The equations governing the motion of the filament in a time interval from $t = 0$ to t, may be obtained by seeking a stationary point of the action integral $J =$
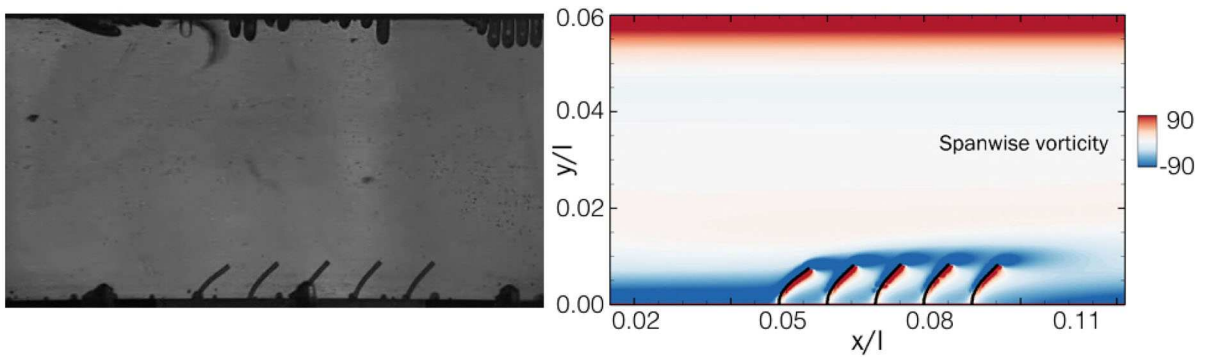
Fig. 1 Snapshot showing the position of the flexible filaments in an oscillating channel flow. *Left* experiments (shadowgraph), *right* numerical results with colour contours of non-dimensional spanwise vorticity, $60\omega_z l/U_{max}$. The channel is filled with glycerine (kinematic viscosity: $1\,cm^2\,s^{-1}$) oscillates at 1 hz matching the filament natural frequency. Channel maximum velocity: $60\,cm\,s^{-1}$; filaments Young modulus: 1.23 MPa; filament size: $D = 1\,mm$, $l = 10\,mm$

$\int_0^t \mathcal{L} dt$ (where $\mathcal{L}$ is the Lagrangian of the system [5]) and reads as:

$$\Delta\rho \frac{\partial^2 \mathbf{X}}{\partial t^2} = (T\mathbf{X}_s)_s - K_B \mathbf{X}_{ssss} + \Delta\rho\mathbf{g} - \epsilon\rho_f \mathbf{F}_{ib}, \qquad (3)$$

where we have used the subscript s to indicate the spatial derivative along the parametric coordinate s defined along the filament. $\Delta\rho$ is the difference in density per unit area of filament cross section between the filament and the fluid. A non-dimensional form of the filament dynamic equation can be obtained by multiplying all terms by $L/(\Delta\rho U_\infty^2)$, ($U_\infty$ being the undisturbed velocity of the fluid flow). The reference quantities used for non dimensionalising the equations are: a reference tension $T_{ref} = \Delta\rho U_\infty^2$, the reference bending rigidity $K_{Bref} = \Delta\rho U_\infty^2 L^2$ and the reference Lagrangian forcing $F_{ref} = \frac{\Delta\rho}{L\epsilon\rho_f} U_\infty^2$. Indicating with Ri is the Richardson number $Ri = gL/U_\infty^2$, the resulting dimensionless equations read:

$$\frac{\partial^2 \mathbf{X}}{\partial t^2} = (T\mathbf{X}_s)_s - K_B \mathbf{X}_{ssss} + Ri\frac{\mathbf{g}}{g} - \mathbf{F}_{ib} \qquad (4)$$

to be solved in $(X(s,t), Y(s,t), Z(s,t))^T$ displacements and in the tension T that plays the role of a Lagrangian multiplier to satisfy the in-extensibility constraint $\mathbf{X} \cdot \mathbf{X} = 1$. Concerning the numerical implementation, following [6]'s formulation we discretise the Eq. 4 together with the in-extensibility condition with second order centered finite differences on a staggered, uniform one dimensional grid where the tension is collocated in the centre of each interval.

The final set of discretised equations reads:

$$\frac{\mathbf{X}^{n+1} - 2\mathbf{X}^n + \mathbf{X}^{n-1}}{\Delta t^2} = [D_s(T^{n+1}D_s\mathbf{X}^{n+1})]$$
$$- K_B D_{ssss}\mathbf{X}^n + Ri\frac{\mathbf{g}}{g} - \mathbf{F}^n \qquad (5)$$

$$D_s\mathbf{X}^{n+1} \cdot D_s\mathbf{X}^{n+1} = 1 \qquad (6)$$

where D_s refers to the standard second order centered finite difference derivative approximation (i.e., $D_{s_i}(q) = (q(s_{i+1}) - q(s_{i-1}))/2\Delta s$). At each time step, the resulting non linear system of equations is solved via a Newton–Raphson method using the exact Jacobian.

2.2 Baseline validation

The immersed boundary method that has been used to model the fluid-elastic flap/filament interactions has been validated in a previous set of two dimensional numerical experiments involving an underlying lattice Boltzmann solver and the same immersed boundary technique employed for the results that will be introduced and discussed in the manuscript. In particular, the two dimensional flapping flag problem and the interaction between flapping flags has been extensively validated against previous soap film
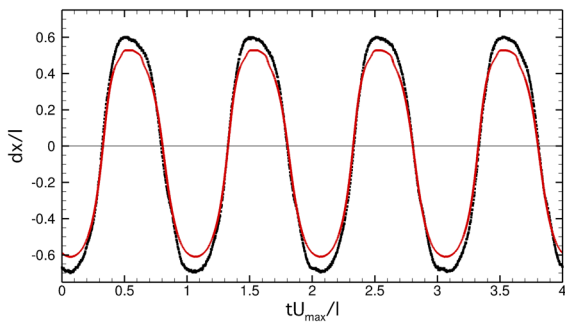
Fig. 2 The streamwise displacement of the tip of the last filament at the right end of the row (see Fig. 1) with respect to time. *Black symbols* are measurements and *red line* is the simulation. (Color figure online)

experiments and numerical simulations (detailed descriptions of the benchmark experiments and of the obtained results are given in [5]).

To determine the predictive capability of the method when dealing with fluid slender structure interactions in three dimensions, an ad-hoc controlled experiment has been carried out considering a pulsating flow within a square section cylinder filled with glycerine (kinematic viscosity: $v = 1\,\mathrm{cm^2\,s^{-1}}$). A row of 5 slender flexible cylindrical elements (cylinder diameter: $D = 1\,\mathrm{mm}$; length $l = 10\,\mathrm{mm}$) has been mounted vertically on the centre-line of the bottom wall of the test section to minimise the effect of the lateral end-walls. The pulsating frequency of the channel has been set to 1 hz (channel maximum velocity: $60\,\mathrm{cm\,s^{-1}}$), nominally matching the filaments natural frequency (filaments Young modulus: 1.23 MPa). The filaments were fabricated by casting an Elastomere (PDMS) in thin holes that are formed by two halves of a mold. After curing at room temperature, the base layer with the filaments can be removed out of the molds. Then the base layer with the filaments is placed flush with the bottom wall of the flow channel so that the filament are perpendicular to the flow direction in zero-flow conditions. The forces acting on the filaments in flow bend the structures which is recorded by a camera.

Figure 1 shows an instantaneous snapshot that compares the numerically obtained results and a shadowgraph visualisation. More quantitative comparison are provided in Fig. 2 showing the streamwise displacement of the tip of the last filament at the right side with respect to time. The frequency of oscillation and the magnitude of displacement in simulation

match the experimental data. The small difference in the amplitude is due to the difference in the boundary conditions used at the base of filaments; in simulations filaments are clamped normal to the wall, however as shown in Fig. 1 this is not fully satisfied in experiments allowing filaments to bend more. Further validation of the fluid structure interaction numerical approach can be found in one of the contributions of the present special issue.

3 Results

We here review all the results that have been obtained during our simulation campaign focusing on the passive control of wakes via the use of flexible slender splitter plates (in two dimensions) and flexible elongated filaments (in three dimensions).

Before tackling the control of bluff body wakes using arrays of deformable devices, we first address the classical and canonical case of a 2D forced mixing layer [14]. This flow encapsulates some of the common features of wake flows including the growth of large vortical structures stemming from an underlying convective instability.

3.1 Altering the vortex pairing process in a mixing layer

Turbulent mixing layers are formed when two co-flowing streams of fluid moving at different velocities come together. This flow configuration is of wide practical interest and plays a significant role, directly or indirectly, in many more complex flows; most of which involve the synthesis of wall bounded flow with a free shear layer of some form [18]. For the case of natural plane mixing layers, vortices form and merge at random downstream positions. The subsequent interaction of these structures leads to an increase of the wake thickness behind the bluff body, which is directly related to the induced from drag. However, when they are forced by an external means, the merging and pairing of the vortices becomes localized, such that events occur at fixed spatial intervals as a function of the forcing. Thus, the coherent structures are locked to the forcing frequency.

In view of our objective to investigate the flow control potential of passive compliant structures, a simple flow such as a forced mixing layer provides a

perfect platform to analyse the affect of a filament on the evolution of the wake. A study of the interaction of a flexible filament in a forced mixing layer is reported below to provide insight into the vortex dynamics and the formation and control of coherent structures.

In the first instance, the mixing layer is formed by applying a hyperbolic tangent mean velocity profile at the inlet. The time-averaged streamwise and cross-stream velocity profiles of a 2D mixing layer are given as:

$$\bar{u}(y) = 1 + \lambda \tan h(y/2), \quad \bar{v}(y) = 0 \qquad (7)$$

where λ is the shear rate defined as $\lambda = \Delta U / 2\bar{U}$. The mean velocity $\bar{U}$ is the average of the high-speed (U_H) and low-speed streams (U_L), and ΔU is the velocity difference between the two streams. The forcing of the mixing layer is often based on the linear stability theory (LST) where the fundamental instability is known to be 2D. Michalke [12] had computed the most unstable mode of the tangential hyperbolic velocity profile using LST and obtained a temporally oscillating perturbation. This time-dependent forcing is super-imposed on the inflow mean velocity to excite the mixing layer. When the mixing layer is forced by a single (fundamental) mode, the shear layer roll-up into spanwise rollers, each separated by a distance of one wavelength. The inflow forcing used in this study is given by [8], which mimics the profiles given by LST. Thus, the instantaneous inflow velocity is given as:

$$u_{in}(y) = \bar{u}_{in}(y) + \epsilon[f(y)\sin(\omega t + \gamma)], \quad v_{in}(y) = 0 \qquad (8)$$

where ϵ is the forcing amplitude, ω is the forcing frequency, and γ is the phase difference between the
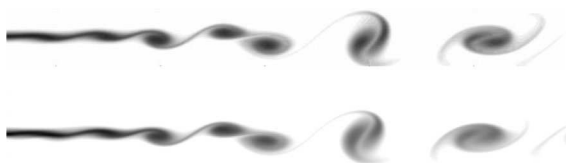

Fig. 3 Instantaneous snapshots of spanwise vorticity distribution: results from [8] (*top*) and current DNS (*bottom*)

discrete forcing modes which is zero as a single fundamental mode is employed. The function $f(y)$ is chosen to be a combination of a cosine function and a decaying function as,

$$f(y) = \cos(ny)\big(1 - \tan h^2(y/2)\big), \qquad (9)$$

where wavelength (n) and the forcing frequency (ω) are tuned according to the LST and the most unstable mode of forcing is found to be at $\omega = 0.22$ and $n = 0.4\pi$ [12].

We first conducted a validation exercise by comparing results from the present numerical code with those from [8]. Figure 3 demonstrates a close correspondence between the instantaneous span-wise vorticity contours from the current DNS and the results of [8]. There is a streamwise offset but Ko et al. do not provide details of the start position and the focus here is on the roll-up mechanism. Table 1 provides the details of the domain size and grid resolution used for this simulation.

Subsequently, the challenge consists of delaying the instability and the vortex pairing process using a flexible filament pinned at the virtual end point of the splitter plate. As a representative case, Fig. 4 shows the effect of filament stiffness on the evolution of coherent structures in a forced mixing layer. It can be seen that when the filament stiffness is tuned to match the forcing frequency of the flow (corresponding to the the most unstable linear eigenvalue), the structures roll-up and lock-in before pairing due to the action of the second frequency (top panel in Fig. 4).

Qualitatively, this means that the growth rate of the mixing layer is reduced for a longer downstream distance (linear growth rate in the region of lock-in coherent structures) and the swaying of the vortices between the high-speed and the low-speed fluid streams is stabilised by the action of the filaments and it takes longer for the sub-harmonic excitation to kick-in.

On the other hand, when the filament stiffness is tuned in a way that its natural frequency is half the forcing frequency, the evolution of the coherent structures is not quite clear and they seem to sway

Table 1 Simulation parameters for forced mixing layer

Domain size	Resolution	ϵ	$(\Delta x)_{min}$	$(\Delta y)_{min}$	Time step
$(360 \times 150)\theta_{in}$	3584×2048	$10\%\ \bar{U}$	0.1	0.002	0.0008

Fig. 4 Instantaneous snapshots showing the position of the flexible filaments in a forced mixing layer, together with the iso-vorticity distributions. *Top panel* natural frequency of the filament matching the first, most unstable mode; *bottom panel* softer filament, its natural frequency matches half of the most unstable mode
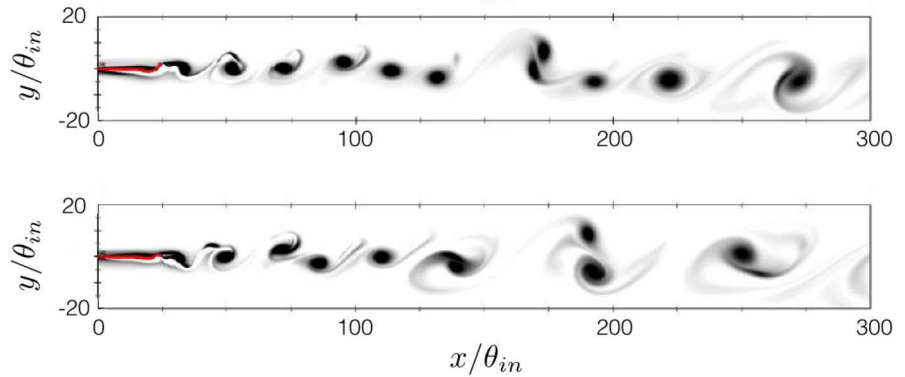
between the two streams before merging albeit with delayed vortex merging than the case without any filament (bottom panel in Fig. 4). Further investigations are underway to investigate the effect of the filament stiffness in a plane forced mixing layer and the related passive control strategies that can be used to anticipate or delaying pairing (i.e., mixing).

3.2 Manipulation of a cylinder wake

To study the possibility of controlling bluff body generated wakes, we have chosen another classical well documented scenario: an uniform stream past an infinite circular cylinder at moderate Reynolds numbers. We have considered both the control of mean drag and lift/drag fluctuations by interacting with the

Fig. 5 The position of the pair of filaments

mean two dimensional wake, and the delay of three dimensional wake transition. For the both cases we have exploited the dynamic response of elastic filaments and splitter plates mounted on the lee side of the cylinder: their capacity of reshaping and instantaneously change the boundary conditions seen by the flow.

3.2.1 Manipulation of a two dimensional cylinder wake

To manipulate and control the 2D wake, we have considered the configuration given in Fig. 5: two filaments placed symmetrically (with respect to the centre line) at various azimuthal angles θ.

Apart from θ, the other degrees of freedom that have been considered were: the filaments lengths, their natural frequencies and the undisturbed flow Reynolds number. The results of the parametric study (i.e., C_D vs. C_L) are given in Fig. 6 for the case in which the filament length is equal to the diameter and the shedding frequency is set to be equal to the filaments natural frequency.

From the figure, it appears clearly that the optimal separation θ (the one that minimises drag and forces fluctuations) is of about $\theta = 15°$ for both the Re_D that have been considered ($Re_D = U_\infty D/v = 200$ and $Re_D = 300$). Increasing further the angle θ, leads to a gradual recover of the forces to the reference values (i.e., without filaments). From the state portrait given in those figures it clearly appears that for values of θ approximately larger than $45°$ the trajectories of $C_D - C_L$ change substantially, this being the symptom of a completely different topology of the vorticity field in the vicinity of the cylinder lee side. It is also interesting to note the symmetry breaking at $\theta = 0°$

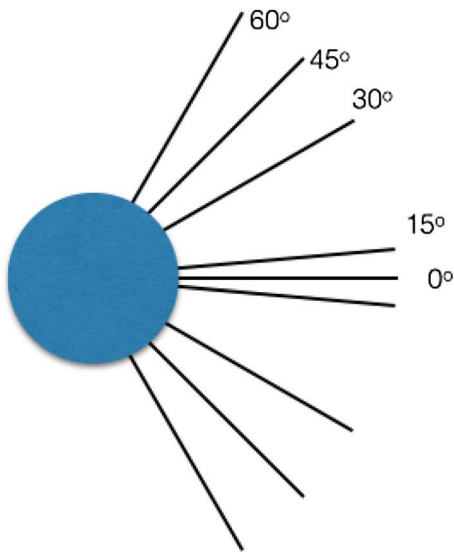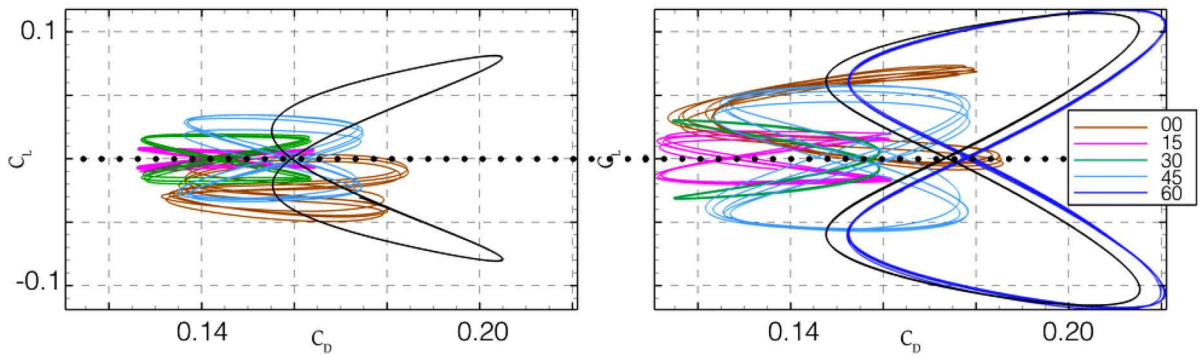**Fig. 6** Lift versus drag coefficients for different separation angles θ between filaments. *Left Re$_D$* = 200; *right Re$_D$* = 300. *Black line* is the reference (i.e., no filament) case. *Brown* is one filament (i.e., $\theta = 0°$). (Color figure online)
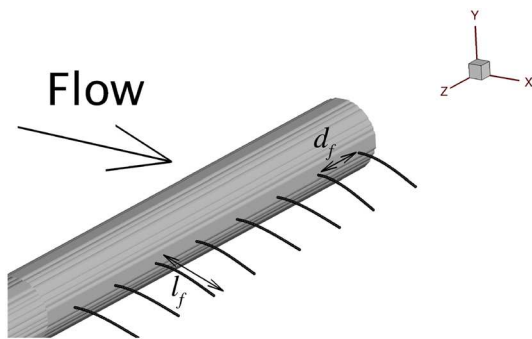

Fig. 7 The considered three dimensional configuration. Two Re_D has been considered $Re_D = 200$ and 300

(i.e., one filament), where the mean lift force is no more zero because the filament gets trapped into the dynamics of one of the separation sides [2].

3.2.2 Delay of three dimensional bifurcation

As a further example on how the wake can be manipulated by passive means based on fluid structure interaction, we have considered the three dimensional transition of the cylinder wake and the eventual possibility of delaying it (increasing the critical Re_D number for which three dimensional transition occurs). The first three dimensional bifurcation occurs with the appearance of an unstable spanwise mode (unstable wavelength of four cylinder diameters) termed as A mode at $Re_D \simeq 188$. When the Reynolds number reaches the value of $Re_D \simeq 259$ another spanwise unstable mode comes into play. This second mode is termed as B mode and is characterised by a shorter critical wavelength (one diameter) [10].
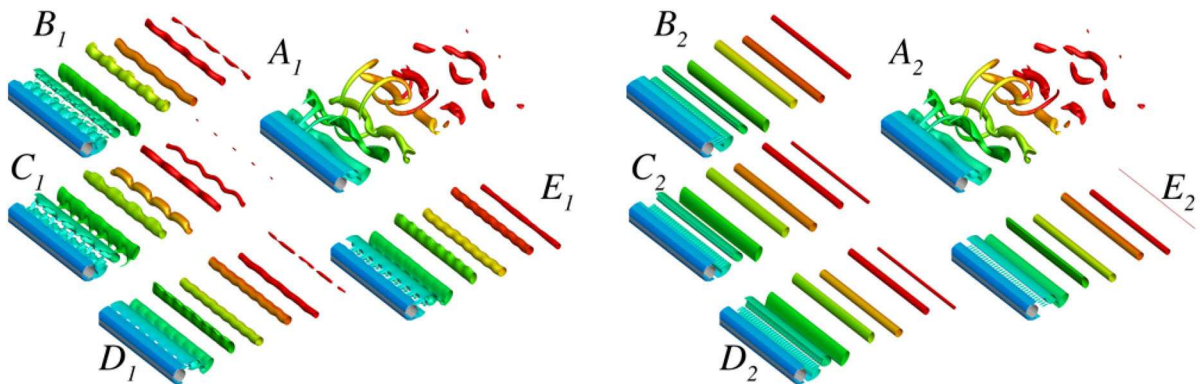

Fig. 8 Isosurfaces of Q criterion at $Re_D = 200$. *Left* spacing between filaments fourth of the unstable mode A ($d_f = D \simeq \lambda_A/4$); *Right* spacing between filaments fourth of the unstable mode B ($d_f = D/4 \simeq \lambda_B/4$). *A1 (A2)* is the case with no filaments, *B1* till *E1* are cases with increasing stiffness, *C1 (C2)* being the resonating case (matched with Strouhal number) and *E1 (E2)* the rigid cases
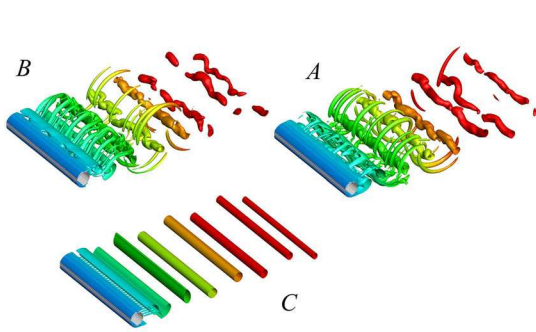
The geometrical configuration that has been initially chosen is sketched in Fig. 7. Also for the 3D case we have carried out a parametric study on the baseline set-up by considering various filaments lengths, stiffnesses, and their spacings in terms of fractions or multiples of the most unstable three dimensional modes wavelengths. The results, in term of wake vorticity structures are summarised in Figs. 8 and 9 for the two Re_D that have been considered: $Re_D = 200$ and $Re_D = 300$ representative of the A and B mode wakes respectively. From both figures, it appears that when the filaments are placed at a distance that interfere with the actual most unstable 3D wavelength and with a natural frequency that is either in the range or higher than the natural shedding frequency, (increasing the stiffness from the resonating value on), the vorticity field shows an almost complete two-dimensional behaviour. The right panel of Fig. 9 displaying the frequency content of the lift forces on the cylinder helps in clarifying the mechanism that inhibits (or delay) the three dimensional bifurcation. In particular, the figure shows that for the baseline, unmanipulated case, a wide range of frequency peaks that lie outside of the shedding harmonic and respective sub-harmonics are present. The large number of extrema in the lift spectrum for the uncontrolled case, is mainly due to three dimensional effects and their interaction with the 2D shedding. On the other hand, the spectra associated with the two cases with filaments present a much smoother behaviour with few maxima associated to the main shedding harmonic and the respective sub-harmonics. Since the natural
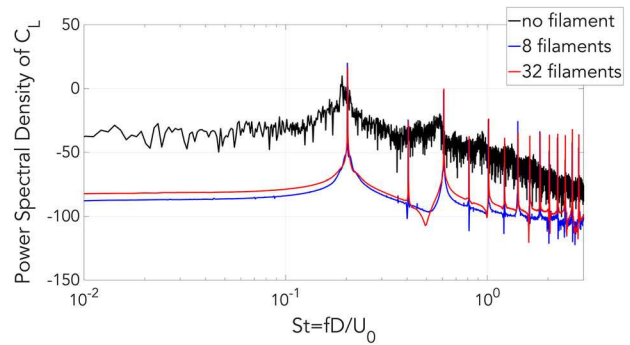
frequency of the filaments is tuned to match the 2D vortex shedding frequency, a possible interpretation of the smooth spectra obtained in the cases with filaments, could be based on an energy redistribution action played by the filaments. The latter being able to collect all energy fluctuations, including the ones associated with 3D motions, and to transfer it back to the main natural oscillation mode of the filaments that corresponds with the two dimensional vortex shedding motion.

Finally, it is worth mentioning that none of the three-dimensional configurations that have been analysed in this work produced a symmetry breaking as observed in the two-dimensional case and as also reported in the experiments conducted by Brosse et al. [3]. However, our study has concerned arrays of rather short filaments as opposed to a single longer filament considered in the mentioned experiments. To asses the range of configurations and conditions that allow for the symmetry breaking to take place in a full three dimensional scenario, more experimental and numerical studies are indeed required and they were not within the scope of the present research.

3.2.3 Simultaneous control of two and three dimensional wake instabilities

Finally, we have also considered the possibility of merging the optimal cases found in the 2D and in the 3D numerical experiments to deliver geometrical configurations able to minimise drag and force fluctuations also delaying the three dimensional transition

Fig. 10 Cylinder covered with two rows of elastic filaments placed at an azimuthal distance of $\theta = 15°$ (*top left panel*). *Right top panel* shows the isosurface of Q at $Re_D = 200$, filaments spacing in the spanwise direction is $d_f = D/4 \simeq \lambda_B/4$. *Bottom panel* $C_L - C_D$ map for the baseline case (*black curve*, no filaments), with filaments (*red curve*). (Color figure online)
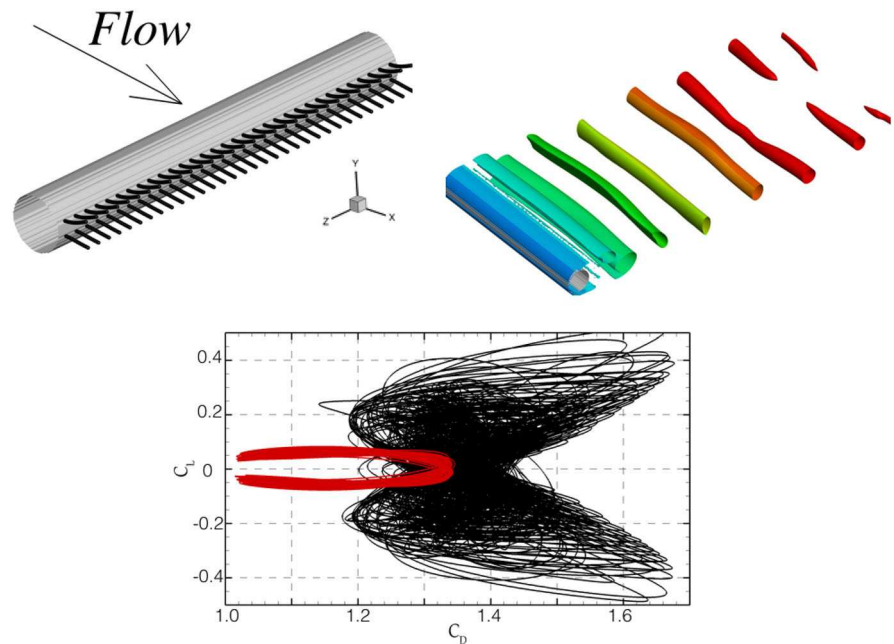
of the wake. The left top panel of Fig. 10 shows the baseline configuration that has been considered: two parallel rows of filaments densely packed in the spanwise direction (distance between filaments one quarter of the mode B), with a length of one diameter and a stiffness value chosen to match the filaments natural frequency with the shedding one. Instantaneous isovalues of Q criterion at $Re_D = 200$ are shown in the right top panel for the aforementioned filament

distribution. The wake topology clearly shows a basically two dimensional vorticity field. The plot at the bottom of the same Fig. 10 displays the $C_L - C_D$ time map at the same Re_D, for the baseline (no filaments) case versus the case with filaments. This last result shows that large reductions in the force coefficients and their fluctuations are achieved with optimal 2D arrangements (Figs. 5, 6) and when the filaments are quite clustered along the span to delay three-dimensional wake transition (Fig. 8).
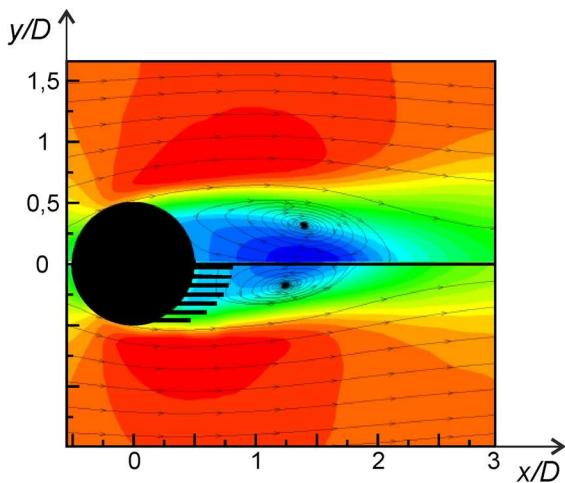
3.3 Control at higher Reynolds-numbers

Up to here the results shown hold for relative moderate Reynolds-numbers of order of O(100) what rises the question of generality of the observed physics for larger range of flow speeds and higher frequencies. This could not be addressed in our numerical simulations so far and therefore experimental studies were carried out to test for the hypothesis of beneficial fluid structure interaction in bluff body flows with attached filaments. The focus is again the wake of a cylinder where flexible structures are attached to the aft part. The details of the experiments are described in [9]. All flow measurements were carried out in a range of Reynolds number $5000 \leq Re_D \leq 31{,}000$ which covers the range where the shedding frequency passes the resonance frequency of the first bending mode.

Fig. 11 Comparison of mean flow field in the wake of a plain cylinder (*top*) and a cylinder covered with hairy flaps (*bottom*) at Re = 27,750
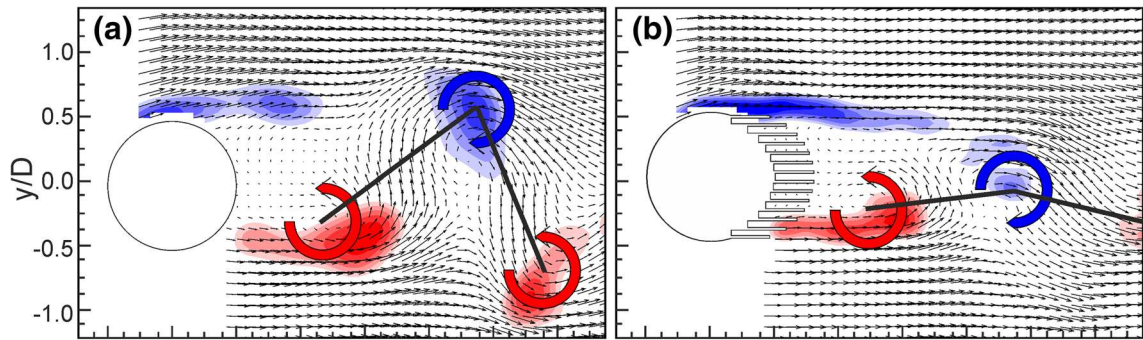
Fig. 12 Comparison of instantaneous PIV vector fields in the wake of a plain cylinder (*left*) and a cylinder covered with hairy flaps (*right*) at Re = 27,750

Figure 11 shows the time averaged flow field around the test cylinders at $Re_D = 27,750$ which is when the shedding frequency is already higher than the resonant peak of the first bending mode. The configurations of hairy flaps (h/H = 1) is compared with the reference cylinder without hairy flaps. The positions and silhouettes of the test cylinders are indicated in black and all velocity information in the shadow region beneath the cylinders are blanked. The results of the PIV measurements show that for the cylinder with hairy flaps the: (i) length of the separation bubble behind the cylinder and its width are decreased; (ii) vortex shedding frequency is increased; (iii) rms-values of the velocity components in streamwise- and transversal-direction are decreased. All these characteristics are connected with a lock-in of the shedding cycle with the resonance frequency of the first bending mode of the hairy-flaps. Accordingly, the shed vortices in the wake are not arranged in a classical Karman-vortex-street style, but they are aligned in a row along the symmetry-axis, see Fig. 12. The analysis of the motions of the hairy-flaps shows that for the resonance the amplitude of the flap-tips are increased up to 0.1D. Combing the results of the PIV measurements with the motion analysis it is found that flow fluctuations are reduced by 42 % in streamwise- and 35 % in transversal direction compared to the reference case of a plain cylinder. The results in the context of the numerical simulation shown herein point out that at higher Reynolds-numbers the same mechanism of wake manipulation. i.e., the lock-in effect, is responsible for the observed decrease in drag.

4 Discussion and conclusions

The reconfiguration capability of many natural systems to adapt to changing aero/hydrodynamic conditions is known since a long time. Examples of such an adaptivity can be found in both the vegetable and animal kingdom: large leaves of trees reshape into conical bodies to protect against strong wing; cactus spines are believed to palliate the form drag of long plants during deserts storms; birds feathers pop up during extreme manoeuvre and the reconfiguring features of seal fur are all well known cases. Common to all these cases is the passive (or believed to be so) but dynamic interaction of the structures with an incoming stream aimed at minimising the generated drag.

Inspired by those observations we have undertaken a number of parametric experiments in two and three dimensions to determine the feasibility of manipulating the wake of bluff bodies by exploiting the interaction of the incoming flow with elongated, elastic (yet no internal damping) filaments or thin membranes attached to the trailing edge of the considered geometry. The individual membranes are extended in spanwise direction to a width of 1 cm. Between successive flaps along the span, a gap of 1 mm has been left so that they can act independently along the whole cylinder.

We have initiated an investigation into the effect of a passive flexible filament in a planar mixing layer, wherein a fundamental excitation imparted by the filament motion was observed to stabilise the mixing layer; locking in coherent structures and thereby

avoiding vortex pairing. When an additional sub-harmonic frequency was applied, the coherent structures were observed to merge due to the action of the sub-harmonic frequency [16]. It is noticed that delivering an understanding of the fluid structure interaction mechanisms underlying this particular case could potentially lead to the development of flow control strategies for thin shear layers. For instance the wake from the trailing edge of an aerofoil at low angle of attack, or the shear layer emanating from the leading edge in aerofoils in deeply stalled conditions.

References

1. Allen J, Smits A (2001) Energy harvesting eel. J Fluids Struct 15(3):629–640
2. Bagheri S, Mazzino A, Bottaro A (2012) Spontaneous symmetry breaking of a hinged flapping filament generates lift. Phys Rev Lett 109:154502
3. Brosse N, Finmo C, Lundell F, Bagheri S (2015) Experimental study of a three-dimensional cylinder–filament system. Exp Fluids 56(6):1–7
4. Fadlun E, Verzicco R, Orlandi P, Mohd-Yusof J (2000) Combined immersed-boundary finite-difference methods for three-dimensional complex flow simulations. J Comput Phys 161:35–60
5. Favier J, Revell A, Pinelli A (2014) A lattice Boltzmann-immersed boundary method to simulate the fluid interaction with moving and slender flexible objects. J Comput Phys 261:145–161
6. Huang WX, Shin SJ, Sung HJ (2007) Simulation of flexible filaments in a uniform flow by the immersed boundary method. J Comput Phys 226(2):2206–2228
7. Kiyoung K, Choi H (1996) Control of laminar vortex shedding behind a circular cylinder using splitter plates. Phys Fluids (1994 Present) 8(2):479–486
8. Ko J, Lucor D, Sagaut P (2008) Sensitivity of two-dimensional spatially developing mixing layers with respect to uncertain inflow conditions. Phys Fluids (1994 Present) 20(7):077,102
9. Kunze S, Brücker C (2012) Control of vortex shedding on a circular cylinder using self-adaptive hairy-flaps. C R Mec 340(1–2):41–56. doi:10.1016/j.crme.2011.11.009
10. Leweke T, Williamson C (1998) Three-dimensional instabilities in wake transition. Eur J Mech B Fluids 17(4):571–586
11. Mazellier N, Feuvrier A, Kourta A (2012) Biomimetic bluff body drag reduction by self-adaptive porous flaps. C R Mec 340(1–2):81–94. doi:10.1016/j.crme.2011.11.006. (Biomimetic flow control)
12. Michalke A (1964) On the inviscid instability of the hyperbolic tangent velocity profile. J Fluid Mech 19(04):543–556
13. Omidyeganeh M, Piomelli U (2011) Coherent structures in the flow over two-dimensional dunes. In: Direct and large-eddy simulation VIII, Springer, Netherlands, pp 245–250
14. Oster D, Wygnanski I (1982) The forced mixing layer between parallel streams. J Fluid Mech 123:91–130
15. Pinelli A, Naqavi I, Piomelli U, Favier J (2010) Immersed-boundary methods for general finite-difference and finite-volume Navier–Stokes solvers. J Comput Phys 229(24):9073–9091
16. Sarkar A, Schlüter J (2014) Large eddy simulations of turbulent mixing layers excited with two frequencies. Flow Turbul Combust 92(3):651–671
17. Taylor G, Burns J, Kammann S, Powers W, Welsh T (2001) Special issue on autonomous ocean-sampling networks-special issue papers—the energy harvesting eel: a small subsurface ocean/river power generator. IEEE J Ocean Eng 26(4):539–547
18. Wilson RV, Demuren A (1994) Numerical simulation of two-dimensional spatially-developing mixing layers. Tech. rep., DTIC Document